COMPARISON OF LANDSAT-9 AND PRISMA SATELLITE DATA FOR LAND USE / LAND COVER CLASSIFICATION

Aylin Tuzcu Kokal[1]*, İrem İsmailoğlu[2], Nebiye Musaoğlu[1,2]

[1] Istanbul Technical University, Civil Engineering Faculty, Department of Geomatics Engineering, 34469 Maslak, Istanbul, Turkey - (tuzcuay, musaoglune)@itu.edu.tr
[2] Istanbul Technical University, Center for Satellite Communications and Remote Sensing, 34469 Maslak, Istanbul, Turkey - (iremism@cscrs.itu.edu.tr)

KEY WORDS: Remote Sensing, Land Use /Land Cover, Landsat-9, PRISMA, Support Vector Machine

ABSTRACT:

Land use and land cover (LU/LC) detection has great significance in management of natural resources and protection of environment. Hence, monitoring LU/LC with the state-of-the-art approaches has gained importance during the recent years and free access satellite images have become valuable data source. The aim of this study is to compare classification abilities of Landsat-9 and PRISMA satellite images while applying Support Vector Machine (SVM) algorithm to distinguish different LU/LC classes. For this purpose, the study area was chosen to be of heterogeneous character that includes industrial area, roads, residential area, airport, sea, forest, vegetation and barren land. When the classification results were visually examined, it was seen that forest, industrial area and airport classes were distinguished more accurately than other classes. On the other hand, qualitative results were validated with quantitative accuracy assessment results. The overall accuracy (OA) and Kappa coefficient values were calculated as 89.33 and 0.88 for Landsat-9 satellite image and as 92.33 and 0.91 for the PRISMA satellite image, respectively. In the accuracy assessment results, although Landsat-9 and PRISMA satellite images showed similar classification performances, a slight improvement was observed by using the PRISMA satellite image. The findings indicated that although both of the Landsat-9 and PRISMA satellite images were proper data to assess the LU/LC of the complex region, a slightly more performance could be achieved by using the PRISMA satellite image.

1. INTRODUCTION

Assessment of the land use and land cover (LU/LC) is playing a vital role for natural resource management and environmental protection (Tan et al., 2016; Tadese et al., 2020). Mapping the LU/LC accurately by using state-of-the-art approaches has become a major focus as it has profound impact on the ecosystem (Huang et al., 2020; Ge et al., 2020). Earth observation satellite imagery have started to provide rich information with the rapid development of remote sensing technologies (Du et al., 2012; Ge et al., 2020; Tong et al., 2020). In particular, remote sensing-based images that were based on a free access policy are the major data source for assessing the spatial extents of various LU/LC classes in a cost and time effective way (Mugo et al., 2020; Nguyen et al., 2020; Tadese et al., 2020; Weigand et al., 2020).

Landsat, which is a joint mission of The National Aeronautics and Space Administration (NASA) and US Geological Survey (USGS), provides consistent multispectral images over the past five decades. Landsat- 9, which was launched in September 2021, is the latest of Landsat Earth-observing satellites series. Although free and open Landsat satellite images provide opportunities for LU/LC applications, multispectral satellite images have some limited factors to classify heterogeneous regions. Thus, the need arises to discriminate complex LU/LC classes by using satellite images that have higher spectral resolution. Hyperspectral satellite images offer a great number of spectral bands that enable acquiring continuous spectral reflectance of the objects on the earth (Tan et al., 2005; Velez-Reyes et al., 2006; Vangi et al., 2021). PRecursore IperSpettrale della Missione Applicativa (PRISMA), which is a mission of Italian Space Agency (ASI), is a new hyperspectral earth observation satellite provides free products and helps to improve the understanding of environment with its high spectral resolution. High accuracies were achieved by using PRISMA satellite image in different classification applications such as detection of non-photosynthetic vegetation (Pepe et al., 2020), different forest types (Vangi et al., 2021), and burned areas (Lazzeri et al., 2021) due to providing narrow spectral bands (≤12 nm).

Numerous studies about usage of previous Landsat satellite images for LU/LC classification applications have been conducted (Coulter et al., 2016; Chen et al., 2020; Deng et al., 2019; Kumar et al., 2021). Landsat-9 satellite has the same technical properties with the Landsat-8 satellite (Url-1). As Landsat-9 is a recently launched satellite, LU/LC classification applications with Landsat-9 satellite image have not yet been extensively performed. On the other hand, PRISMA satellite images were widely used in studies on discriminating different types of land cover classes (Lazzeri et al., 2021; Vangi et al., 2021). However, there is a lack of studies about discriminating different LU/LC types by using PRISMA satellite image.

Comparison of classification performances of Landsat-9 and PRISMA satellite images which bear the same spatial resolution was aimed in this study for determining different LU/LC classes.

* Corresponding author

For this purpose, hyperparameters of the Radial Basis Function (RBF) kernel were tuned and pixel- based support vector machine (SVM) which is a machine learning classifier, was applied. In addition to qualitative accuracy assessment, quantitative analysis was also conducted based on error matrices, and accuracy metrics were calculated.

2. DATA AND METHODOLOGY

2.1. Study Area

The pilot area of approximately 125.85 km^2 is located in Çanakkale Province (Turkey) was selected as the study area and depicted in Figure 1. The reason for selecting the pilot area was that it consists diverse LU/LC classes like industrial area, roads, residential area, airport, sea, forest, vegetation and barren land. The secondary reason of that selection is that acquisition of Landsat-9 and PRISMA satellite images on the same day.

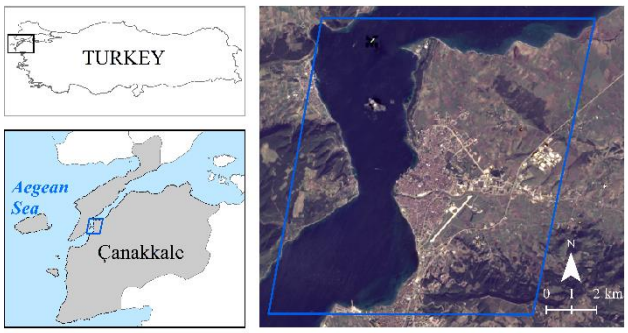

Figure 1. Upper left image belongs the map of Turkey, lower left image belongs to the map of Çanakkale Province, right image belongs to the Landsat-9 image true color composite, which was acquired on 18.01.2022, of the geographical location of the study area.

2.2 Data Used

The study was based on two different types of satellite data for assessing the contribution of the spectral resolution on the accuracy of LU/LC classification results. Hence, as satellite images which were acquired on the same day and have the same spatial resolution were selected. Landsat-9 and PRISMA satellite images were acquired on 18.01.2022 and included 11 and 235 spectral bands with 30-m spatial resolution, respectively. Technical specifications of the PRISMA and Landsat-9 satellite images are shown in Table 1 (Url-2) and Table 2 (Url-1; Url-3; Url-4), respectively.

Swath Width (km)	30
Ground Sample Distance (m)	Hyperspectral : 30 PAN : 5
Spectral Coverage (nm)	VNIR: 400 – 1010 SWIR: 920 – 2500 PAN: 400 – 700 nm
Spectral Resolution	240 bands (bandwidth: ≤12 nm)
Temporal Resolution	Approximately 29 days

Table 1. Data specifications of the PRISMA satellite images (Url-2).

Swath Width (km)	185
Ground Sample Distance (m)	Multispectral : 30 PAN : 15
Spectral Coverage (nm)	430 - 2290
Spectral Resolution	9 bands (bandwidth: 20-180 nm)
Temporal Resolution	16 days

Table 2. Data specifications of the Landsat-9 Operational Land Imager 2 (OLI-2) Instrument (Url-1; Url-3; Url-4).

2.3 Methodology

This research consists of several steps, which are presented in a flow chart. (Figure 2). The details of the methods are explained in this section.

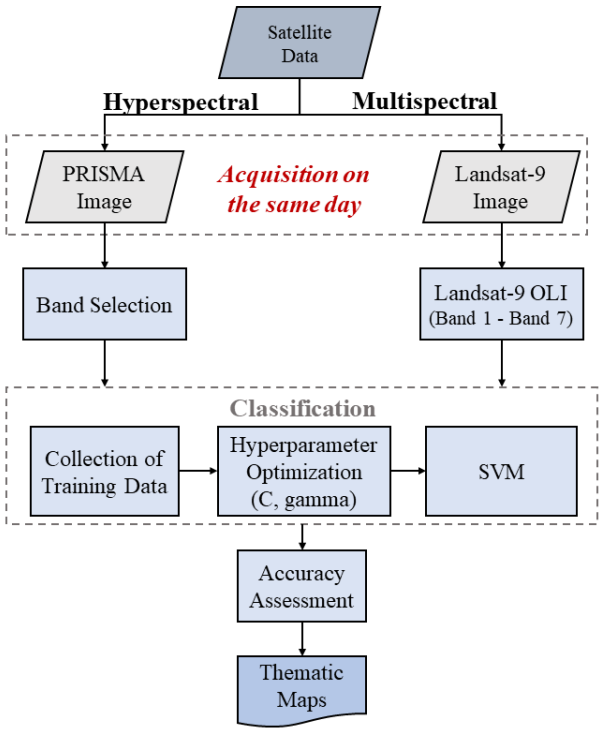

Figure 2. The flow chart of the methodology used.

Since, Landsat-9 Level-2 satellite image and PRISMA Level 2D satellite images that have been atmospherically corrected were used, no further atmospheric correction was applied to the satellite images. Some of the spectral bands (1-5, 13-15, 20-21, 35-37, 56-63 of VNIR Bands; 42-49, 168-173 of SWIR Bands) of PRISMA satellite image that included high level of noise were eliminated. The composite image was generated from the selected proper spectral bands and defined as input data at the PRISMA image classification stage. On the other hand, coastal, blue, green, red, near infrared, shortwave infrared 1 and shortwave infrared 2 of Landsat-9 image were defined as input data at the Landsat-9 image classification stage. Ships and clouds were masked in the satellite images. Radial Basis Function kernel SVM (Vapnik, 1979; Vapnik, 2013) that is a supervised machine learning algorithm and also a powerful classifier (Khatami and Mountrakis, 2012; Rana and Suryanarayana, 2020) was preferred to discriminate the complex classes. As a first step training dataset was collected in the classification stage. In the next step,

hyperparameters of the SVM classifier, which are cost and gamma parameters, were optimized (Mountrakis et al., 2011) by using grid search method (Pedregosa et al., 2011). By using optimized hyperparameters, SVM algorithm was applied to these multispectral and hyperspectral satellite images to discriminate different LU/LC classes.

In assessing the accuracies of the results that were obtained by using PRISMA and Landsat-9 satellite images, quantitative and qualitative analysis were performed. Error matrices were generated based on 300 test points to calculate accuracy assessment metrics of OA, kappa coefficient, producer's and user's accuracy, and the classification results were evaluated quantitatively. Error matrices of the classification results that were obtained by using Landsat-9 and PRISMA satellite images are shown in Table 3 and Table 4, respectively.

Class ID		Reference Data							
		V.	A.	F.	S.	I.A.	R.	R.A.	B.L.
Classified Data	V.	**41**	0	0	0	0	0	0	3
	A.	0	**30**	0	0	6	1	0	0
	F.	1	0	**36**	0	0	0	0	0
	S.	0	0	3	**33**	0	0	0	0
	I.A.	0	2	0	0	**28**	3	1	0
	R.	0	0	0	0	1	**31**	1	0
	R.A.	0	0	0	0	0	1	**31**	0
	B.L.	1	0	0	0	0	1	7	**38**

Table 3. The error matrix of the classification result that was obtained by using Landsat-9 satellite image (V: Vegetation, A: Airport, F: Forest, S: Sea, I.A.: Industrial Area, R: Road, R. A.: Residential Area, B. L.: Barren Land).

Class ID		Reference Data							
		V.	A.	F.	S.	I.A.	R.	R.A.	B.L.
Classified Data	V.	**41**	0	0	0	0	0	1	3
	A.	0	**31**	0	0	5	0	0	0
	F.	0	0	**38**	0	0	1	0	0
	S.	0	0	1	**33**	0	0	0	0
	I.A.	0	1	0	0	**28**	2	0	0
	R.	2	0	0	0	2	**32**	2	0
	R.A.	0	0	0	0	0	2	**37**	1
	B.L.	0	0	0	0	0	0	0	**37**

Table 4. The error matrix of the classification result that was obtained by using PRISMA satellite image (V: Vegetation, A: Airport, F: Forest, S: Sea, I.A.: Industrial Area, R: Road, R. A.: Residential Area, B. L.: Barren Land).

3. RESULTS AND CONCLUSIONS

The LU/LC maps that were produced by applying SVM to Landsat-9 and PRISMA satellite images were shown in Figure 3 and Figure 4, respectively.

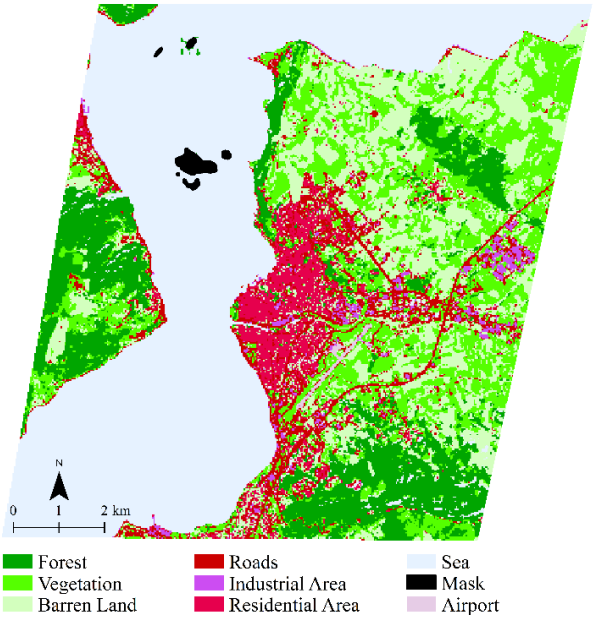

Figure 3. The LU/LC map that was produced by applying SVM to Landsat-9 satellite image.

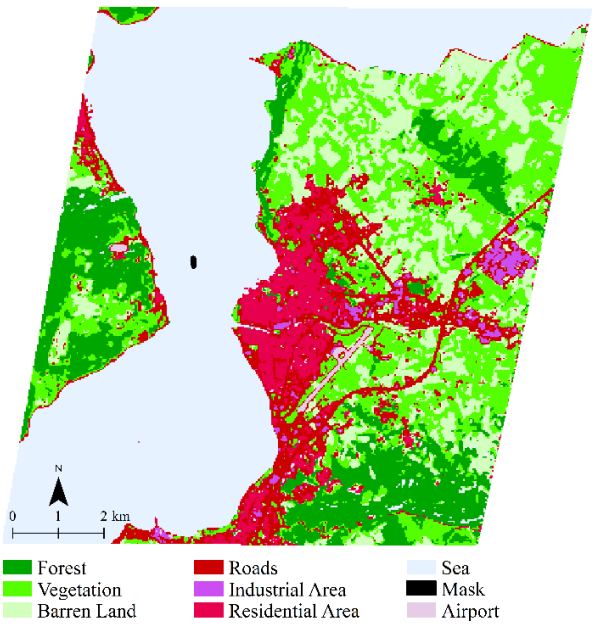

Figure 4. The LU/LC map that was produced by applying SVM to PRISMA satellite image.

In the visual analysis (Figure 5), Google Earth images (Figure 5.a, 5.d, 5.g) were used as reference data. It was observed that the airport was discriminated more accurately in the classification result (Figure 5.b), which was retrieved from the PRISMA satellite image, than the classification result (Figure 5.c) which was retrieved from the Landsat-9 satellite image. Similarly, industrial area was distinguished more accurately by using PRISMA image (Figure 5.h), (Figure 5.i). On the other hand, roads were classified more accurately with Landsat-9 satellite image as shown in Figure 5.f, compared to PRISMA classification result that is shown in Figure 5.e.

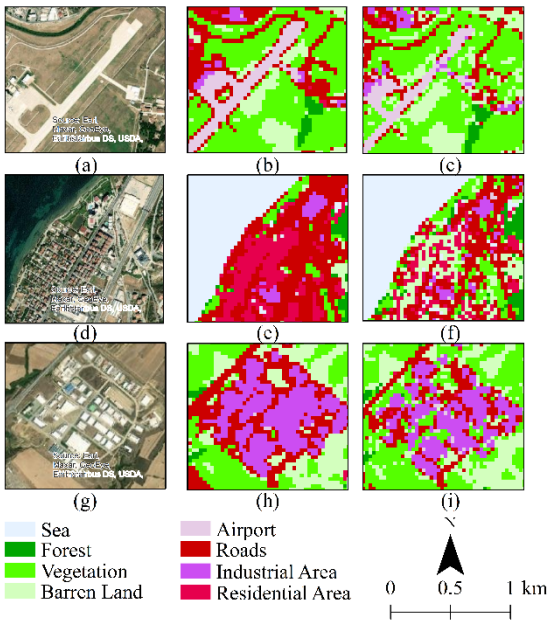

Figure 5. Magnified images of a, d, g reference maps; b, e, h the classification results that were obtained by PRISMA satellite image; c, f, i the classification results that were obtained by Landsat-9 satellite image.

Kappa coefficient values of the SVM classification results obtained from Landsat-9 and PRISMA were calculated as 0.88 and 0.91, OAs were calculated as 89.33% and 92.33% respectively. The accuracy assessment results are given in Table 5.

Classes	LANDSAT-9		PRISMA	
	U.A.	P.A.	U.A.	P.A.
Vegetation	93.18	95.35	91.11	95.35
Airport	81.08	93.75	86.11	96.88
Forest	97.30	92.31	97.44	97.44
Sea	91.67	100.00	97.06	100.00
Industrial Area	82.35	80.00	90.32	80.00
Road	93.94	83.78	84.21	86.49
Residential Area	96.88	77.50	92.50	92.50
Barren Land	80.85	92.68	100.00	90.24
OA (%)	89.33		92.33	
Kappa	0.88		0.91	

Table 5. The results of the accuracy assessment metrics.

In the accuracy assessment results, similar results were obtained from these two different classifications. However, due its higher spectral resolution, the classification capability of the PRISMA satellite image was observed as slightly higher than the Landsat-9 satellite image.

ACKNOWLEDGEMENTS

This study was carried out using PRISMA Products, © of the Italian Space Agency (ASI), delivered under an ASI License to use. The authors would like to acknowledge the financial support of Istanbul Technical University Scientific Projects Office (BAP) under project number MDK-2021-43054 and also to The Scientific and Technological Research Council of Turkey (TÜBİTAK) Project under project number 121G142.

REFERENCES

Chen, C., Chen, H., Liao, W., Sui, X., Wang, L., Chen, J., Chu, Y., 2020. Dynamic monitoring and analysis of land-use and land-cover change using Landsat multitemporal data in the Zhoushan Archipelago, China. *IEEE Access*, 8, pp. 210360-210369.

Coulter, L. L., Stow, D. A., Tsai, Y. H., Ibanez, N., Shih, H. C., Kerr, A., Benza, M., Weeks, J.R., Mensah, F., 2016. Classification and assessment of land cover and land use change in southern Ghana using dense stacks of Landsat 7 ETM+ imagery. *Remote Sensing of Environment*, 184, pp. 396-409.

Deng, Z., Zhu, X., He, Q., Tang, L., 2019. Land use/land cover classification using time series Landsat 8 images in a heavily urbanized area. *Advances in Space Research*, 63(7), pp. 2144-2154.

Du, P., Xia, J., Zhang, W., Tan, K., Liu, Y., Liu, S., 2012. Multiple classifier system for remote sensing image classification: A review. *Sensors*, 12(4), pp. 4764-4792.

Ge, G., Shi, Z., Zhu, Y., Yang, X., Hao, Y., 2020. Land use/cover classification in an arid desert-oasis mosaic landscape of China using remote sensed imagery: Performance assessment of four machine learning algorithms. *Global Ecology and Conservation*, 22, e00971.

Huang, Z., Qi, H., Kang, C., Su, Y., Liu, Y., 2020. An ensemble learning approach for urban land use mapping based on remote sensing imagery and social sensing data. *Remote Sensing*, 12(19), 3254.

Khatami, R., Mountrakis, G., 2012. Implications of classification of methodological decisions in flooding analysis from hurricane Katrina. *Remote Sensing*, 4(12), pp. 3877–3891.

Kumar, P., Dobriyal, M., Kale, A., Pandey, A.K., 2021. Temporal dynamics change of land use/land cover in Jhansi district of Uttar Pradesh over past 20 years using Landsat TM, ETM+ and OLI sensors. *Remote Sensing Applications: Society and Environment*, 23, 100579.

Lazzeri, G., Frodella, W., Rossi, G., Moretti, S., 2021. Multitemporal mapping of post-fire land cover using multiplatform PRISMA Hyperspectral and Sentinel-UAV multispectral data: Insights from case studies in Portugal and Italy. *Sensors*, 21(12), 3982.

Mountrakis, G., Im, J., Ogole, C., 2011. Support vector machines in remote sensing: A review. *ISPRS Journal of Photogrammetry and Remote Sensing*, 66(3), pp. 247-259.

Mugo, R., Waswa, R., Nyaga, J. W., Ndubi, A., Adams, E. C., Flores-Anderson, A. I., 2020. Quantifying land use land cover changes in the Lake Victoria basin using satellite remote sensing: The trends and drivers between 1985 and 2014. *Remote Sensing*, 12(17), 2829.

Nguyen, L. H., Joshi, D. R., Clay, D. E., Henebry, G. M., 2020. Characterizing land cover/land use from multiple years of Landsat and MODIS time series: A novel approach using land surface phenology modeling and random forest classifier. *Remote Sensing of Environment*, 238, 111017.

Url-1: https://www.usgs.gov/landsat-missions/landsat-9, retrieved date 19 March 2022.

Url-2: http://prisma.asi.it/missionselect/docs/PRISMA%20Product%20Specifications_Is2_3.pdf, retrieved date 14 April 2022.

Url-3: https://d9-wret.s3.us-west-2.amazonaws.com/assets/palladium/production/s3fs-public/media/files/LSDS-2082_L9-Data-Users-Handbook_v1.pdf, retrieved date 14 April 2022.

Url-4: https://landsat.gsfc.nasa.gov/wp-content/uploads/2020-11/Landsat%209%20brochure%20final%20508%20compliant.pdf, retrieved date 14 April 2022.

Pedregosa, F., Varoquaux, G., Gramfort, A., Michel, V., Thirion, B., Grisel, O., Blondel, M., Prettenhofer, P., Weiss, R., Dubourg, V., Vanderplas, J., Passos, A., Cournapeau, D., Brucher , M., Perrot, M., Duchesnay, E., 2011. Scikit-learn: Machine learning in Python. *The Journal of Machine Learning Research*, 12, pp. 2825-2830.

Pepe, M., Pompilio, L., Gioli, B., Busetto, L., Boschetti, M., 2020. Detection and classification of non-photosynthetic vegetation from PRISMA hyperspectral data in croplands. *Remote Sensing*, 12(23), 3903.

Rana, V.K., Suryanarayana, T.M.V., 2020. Performance evaluation of MLE, RF and SVM classification algorithms for watershed scale land use/land cover mapping using sentinel 2 bands. *Remote Sensing Applications: Society and Environment*, 19, 100351.

Tadese, M., Kumar, L., Koech, R., Kogo, B. K., 2020. Mapping of land-use/land-cover changes and its dynamics in Awash River Basin using remote sensing and GIS. *Remote Sensing Applications: Society and Environment*, 19, 100352.

Tan, K., Wan, Y., Yang, Y., Duan, Q., 2005. Study of hyperspectral remote sensing for archaeology. *Journal of Infrared and Millimeter Waves*, [in Chinese], 24(6), 437-440.

Tan, Y., Bai, B., Mohammad, M. S., 2016. Time series remote sensing based dynamic monitoring of land use and land cover change. In: *2016 4th International Workshop on Earth Observation and Remote Sensing Applications (EORSA)*, Guangzhou, China, pp. 202-206. doi: 10.1109/EORSA.2016.7552797.

Tong, X. Y., Xia, G. S., Lu, Q., Shen, H., Li, S., You, S., Zhang, L., 2020. Land-cover classification with high-resolution remote sensing images using transferable deep models. *Remote Sensing of Environment*, 237, 111322.

Vangi, E., D'Amico, G., Francini, S., Giannetti, F., Lasserre, B., Marchetti, M., Chirici, G., 2021. The new hyperspectral satellite PRISMA: Imagery for forest types discrimination. *Sensors*, 21(4), 1182.

Vapnik, V., 1979. *Estimation of dependences Based on Empirical Data*. [in Russian]. Nauka, Moscow. (English translation: Springer-Verlag, New York).

Vapnik, V., 2013. *The Nature of Statistical Learning Theory*. Springer Science & Business Media, New York.

Velez-Reyes, M., Goodman, J.A., Castrodad-Carrau, A., Jiménez-Rodriguez, L.O., Hunt, S.D., Armstrong, R., 2006. Benthic habitat mapping using hyperspectral remote sensing. *Remote Sensing of the Ocean, Sea Ice, and Large Water Regions*, Stockholm, Sweden, 6360, 63600C1-63600C11. doi: 10.1117/12.692996

Weigand, M., Staab, J., Wurm, M., Taubenböck, H., 2020. Spatial and semantic effects of LUCAS samples on fully automated land use/land cover classification in high-resolution Sentinel-2 data. *International Journal of Applied Earth Observation and Geoinformation*, 88, 102065.